nature geoscience

LETTERS

PUBLISHED ONLINE: 14 MARCH 2016 | DOI: 10.1038/NGEO2670

Disentangling greenhouse warming and aerosol cooling to reveal Earth's climate sensitivity

T. Storelvmo[1]*, T. Leirvik[2], U. Lohmann[3], P. C. B. Phillips[4] and M. Wild[3]

Earth's climate sensitivity has long been subject to heated debate and has spurred renewed interest after the latest IPCC assessment report suggested a downward adjustment of its most likely range[1]. Recent observational studies have produced estimates of transient climate sensitivity, that is, the global mean surface temperature increase at the time of CO_2 doubling, as low as 1.3 K (refs 2,3), well below the best estimate produced by global climate models (1.8 K). Here, we present an observation-based study of the time period 1964 to 2010, which does not rely on climate models. The method incorporates observations of greenhouse gas concentrations, temperature and radiation from approximately 1,300 surface sites into an energy balance framework. Statistical methods commonly applied to economic time series are then used to decompose observed temperature trends into components attributable to changes in greenhouse gas concentrations and surface radiation. We find that surface radiation trends, which have been largely explained by changes in atmospheric aerosol loading, caused a cooling that masked approximately one-third of the continental warming due to increasing greenhouse gas concentrations over the past half-century. In consequence, the method yields a higher transient climate sensitivity (2.0 ± 0.8 K) than other observational studies.

Atmospheric CO_2 concentration is projected to double from pre-industrial levels during this century[1], and constraining Earth's temperature response is a primary objective for designing mitigation and adaptation policies. Whereas substantial attention has been devoted to model estimates of Earth's equilibrium climate sensitivity[4] (that is, the surface temperature response to CO_2 doubling once a new equilibrium climate state has been reached), more relevant to public and policymakers is the temperature change that occurs at the time of CO_2 doubling, known as 'transient climate sensitivity' (TCS; ref. 5). Constraining TCS on the basis of observational records is complicated by the fact that recent climate change was not forced by CO_2 changes alone. Downward solar radiation at the surface (DSRS, measured in W m^{-2}) reported at approximately 1,300 surface stations over the time period 1964–2010 (Fig. 1a,b) exhibits a downward trend in DSRS which is commonly referred to as 'global dimming' (Fig. 1c; ref. 6). The most plausible explanation for global dimming is increased atmospheric aerosol loading derived from anthropogenic burning of fossil fuels and biomass[7]. The overall effect of aerosols increases Earth's albedo, either by direct interaction with solar radiation, or by increasing the lifetime, areal extent, and/or reflectivity of clouds[8]. For some portions of the world, the appearance of regional trends opposing the global negative DSRS trend ('regional brightening') is observed towards the end of the twentieth century, consistent with a reduction in aerosol emissions in much of the developed world[6]. Atmospheric aerosol loading is broadly reflected in global emissions of sulfur dioxide (SO_2), a precursor for sulfate aerosols (Fig. 1c). Sulfate is only one of several aerosol species emitted by human activity, but the relationship between SO_2 emissions and downward solar radiation broadly reflects the impact of anthropogenic atmospheric aerosol loading on global dimming, and thereafter on the weaker patterns of regional brightening. Note that trends in volcanic or solar activity also affect DSRS, and that similar SO_2 emissions may have different radiative effects depending on factors such as latitude and climate regime. Cloudiness also impacts DSRS, but several studies that sought to explain trends in DSRS by changes in cloudiness have concluded that no such relationship could be identified[9]. The fact that a subset of surface stations that can distinguish between clear and cloudy skies show dimming and brightening trends in clear-sky data further points to aerosols as the main driver of DSRS trends[6].

Perturbations to Earth's radiation budget, whether by greenhouse gases or aerosols, are commonly referred to as radiative forcings (RFs, W m^{-2}). Positive RFs exerted by anthropogenic CO_2 imply a net energy gain by the Earth–atmosphere system and subsequent warming, whereas negative RFs exerted by anthropogenic aerosols imply net energy loss. TCS relates the net RF (ΔF) to the change in global mean temperature (ΔT) through the following equation:

$$\mathrm{TCS} = \frac{F_{2x}\Delta T}{\Delta F} \quad (1)$$

where F_{2x} is the forcing due to a doubling of atmospheric CO_2 concentrations. Over the past century, the net forcing has been dominated by the two competing RFs due to long-lived greenhouse gases (GHGs) and aerosols ($\Delta F \approx \Delta F_{\mathrm{GHG}} + \Delta F_{\mathrm{AER}}$; ref. 8). For an observed temperature change, an overestimation of ΔF translates into an underestimation of the TCS (equation (1)), and vice versa[10]. Compared to the RF resulting from GHG increases, the RF associated with aerosol forcing is poorly constrained. Although tremendous progress has been made on the representation of various aerosol processes in global climate models (GCMs), aerosol–cloud interactions remain a major source of uncertainty[8], and the spread in GCM estimates of cloud-mediated and total aerosol effects on climate is almost as wide today as when the field emerged two decades ago[11]. Several studies also suggest that GCMs are generally not able to reproduce the observed global dimming and subsequent regional brightening (for example, ref. 7). Because of the intimate coupling between the uncertain ΔF and TCS (ref. 12), estimates of the TCS simulated by GCMs are considered unreliable. TCS estimates that are independent of GCMs are thus critical for advancing the topic.

[1]Department of Geology and Geophysics, Yale University, New Haven, Connecticut 06511, USA. [2]Graduate School of Business, Nord University, 8049 Bodø, Norway. [3]Institute for Atmospheric and Climate Science, ETH Zurich, 8092 Zurich, Switzerland. [4]Department of Economics, Yale University, New Haven, Connecticut 06511, USA. *e-mail: trude.storelvmo@yale.edu

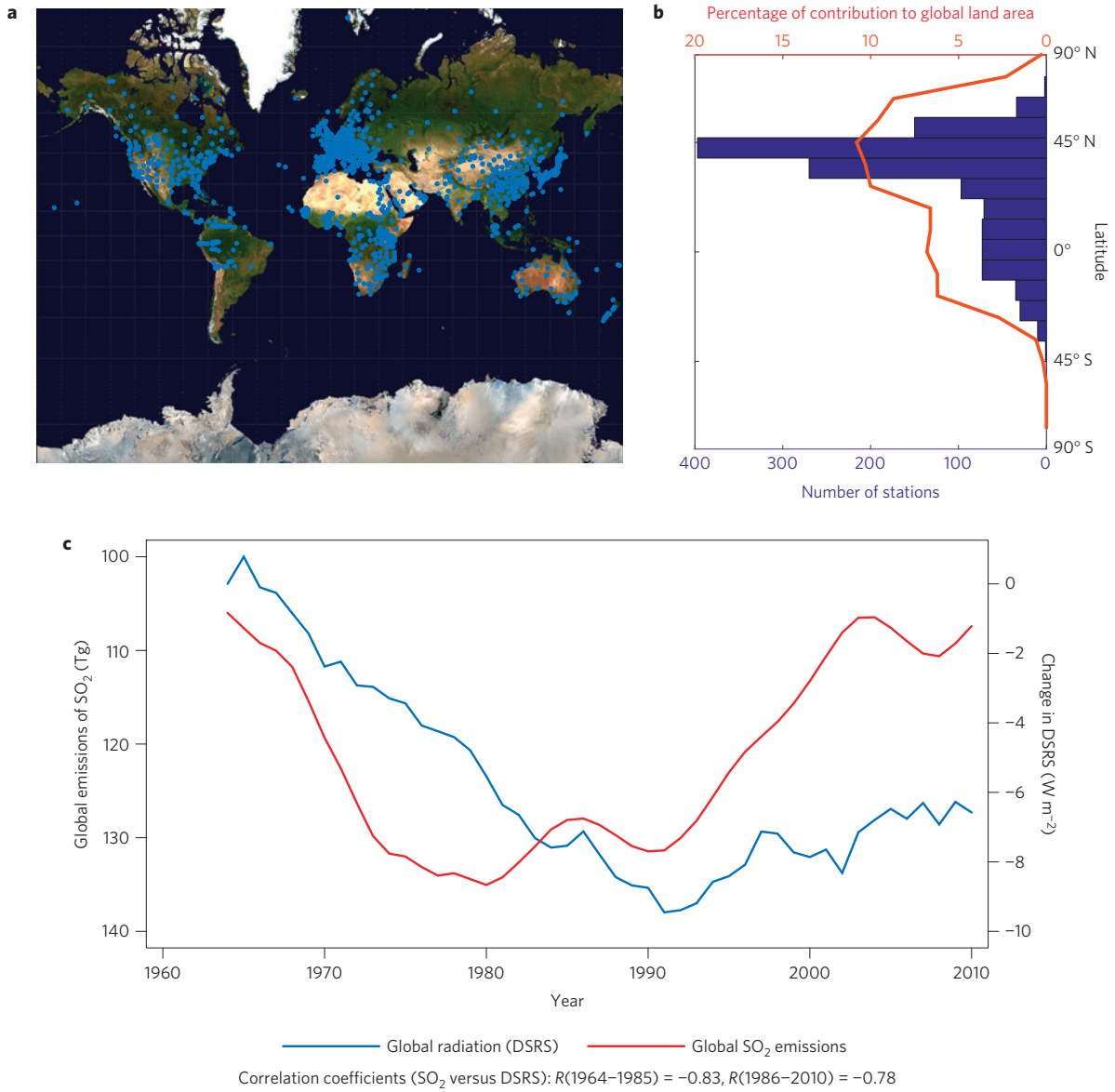

Figure 1 | Radiation measurements from 1,300 surface stations. a, Geographical location of each of the ~1,300 surface stations incorporated in the study. Map courtesy of NASA Earth Observatory. **b**, Number of surface stations (blue bars, bottom axis) and contribution to global land area (Antarctica excluded) (red line, top axis) per 10° latitude band. **c**, The trend in DSRS, shown as the change relative to 1964, calculated by averaging the year-to-year change over all stations shown above (right axis, blue curve). Also shown are global mean emissions of sulfur dioxide, SO_2 (red curve, left axis; refs 28,29), a precursor to sulfate aerosols. Both curves show 5-year running means.

In this study, we estimate TCS by applying surface air temperature observations from the high-resolution (0.5°) data set from the Climate Research Unit (CRU; ref. 13), equivalent CO_2 concentrations ($CO_{2,eq}$, in ppm, see Methods) from the Annual Greenhouse Gas Index (AGGI; ref. 14) and DSRS from the Global Energy Balance Archive (GEBA; ref. 15). Observations from the ~1,300 surface stations considered were used to estimate the free parameters of a set of equations predicting temperature at individual stations as a function of $CO_{2,eq}$ and DSRS, using dynamic panel data methods that allow for potential long-run cointegrating links among component global time series[16] (see Methods). Econometric analysis using cointegration methodology has previously been successfully applied to global mean climate time series, in attempts to link observed climate change to anthropogenic and natural climate forcings (for example, refs 17,18). The present study goes beyond this body of research by applying dynamic panel modelling methods in conjunction with cointegration techniques to assess individual station responses to long-run movements using a rich data set with a spatial as well as temporal dimension, including temperature, $CO_{2,eq}$ and surface radiation. Using this framework, the observed continental temperature evolution from 1964 to 2010 can be reasonably reproduced, and yields a spatially averaged temperature increase of approximately 0.8 K (Fig. 2).

Using the method to calculate temperature evolution under the hypothetical case that $CO_{2,eq}$ remained constant at 1964 values, results in a cooling that reflects the total aerosol effect. Surface cooling is approximately 0.4 K, averaged over the surface stations considered. Conversely, if DSRS is kept constant at 1964 levels, corresponding to constant atmospheric aerosol concentrations, a warming of 1.2 K is calculated. In other words, about one-third of potential continental warming attributable to increased greenhouse gas concentrations has been masked by aerosol cooling during this time period. The masking effect is strongest before 1990, consistent with previous studies for that time period[19]. An important

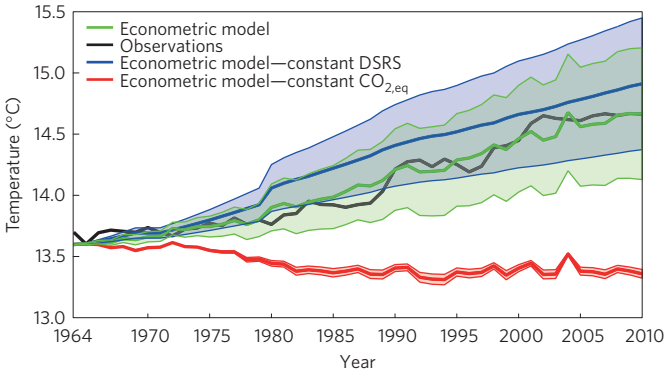

Figure 2 | Temperature trend decomposition. Global land temperature as observed (black curve, CRU TS3.2 data sampled at GEBA stations only, shown as 5-year running mean), and as predicted with equations (2) and (3), given in Methods (green curve). The red curve is calculated using the same framework, but setting $CO_{2,eq}$ concentrations constant at 1964 values, such that the temperature trend is controlled by the DSRS trend alone. Likewise the blue curve shows the temperature predicted with DSRS constant at 1964 values, such that the temperature trend is controlled only by $CO_{2,eq}$. Predicted temperatures are all shown as 5-year running means. Shadings represent the standard error.

consequence of this result is that comparable analyses that fail to account for the aerosol masking will erroneously lead to a TCS that is too low by a factor of approximately two-thirds. This is consistent with a recent GCM analysis suggesting that aerosol forcing (and forcing associated with other short-lived species) yields a disproportionately larger surface temperature response than CO_2 forcing because of the nature and spatial pattern of the forcings[20]. However, note that because the DSRS data set used here provides radiation trends at the surface, as opposed to at the top of the atmosphere where RFs are evaluated, the DSRS change and the resulting cooling found in this study should not be thought of as a traditional forcing–response relationship.

The analysis further yields a best estimate of the TCS of 3.1 K over land, with a 95% confidence interval of 1.7–4.4 K, which is obtained by computing $\gamma_3 \log_2$, where γ_3 is the parameter in equation (3) that controls the sensitivity to $CO_{2,eq}$ (see Methods). We deem this TCS estimate as representative for the global land surface, despite the inhomogeneous spatial coverage of surface stations providing data for the analysis (Fig. 1a); for greenhouse warming, variations with latitude are large and important, whereas variations within a given latitude band are considered of secondary importance. Because the number of surface stations in each latitude band corresponds well with the relative contribution to global land coverage from any given latitude, latitudinal dependence should be well represented (Fig. 1b). Given that land has warmed at exactly double the rate of the ocean over the past century[21], TCS for the entire globe is estimated to be ~2.0 K (95% confidence interval 1.1–2.9 K) (obtained by taking $\mathrm{TCS_{Globe}} \approx \mathrm{TCS_{Land}}\,(f_{\mathrm{Land}} + 0.5 f_{\mathrm{Ocean}})$, where f_{Ocean} and f_{Land} refer to the global land/ocean fractions). A recent analysis used energy budget calculations combined with observations to constrain climate sensitivity[2], but required GCMs for information on radiative forcings. That study reported a 95% confidence interval for TCS based on the time period 1970–2009 of 0.7–2.5 K, and a best estimate of 1.4 K, 0.6 K lower than the best estimate produced by our GCM-independent method. A comprehensive survey of existing

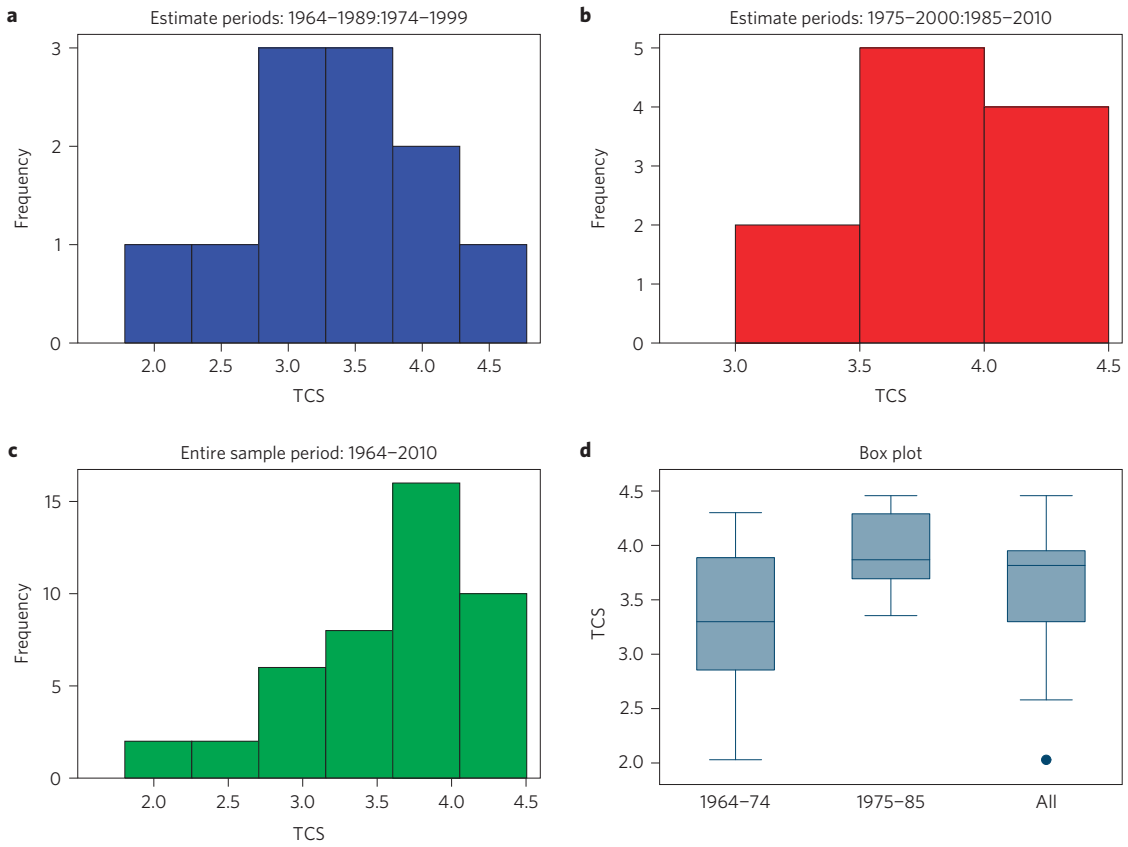

Figure 3 | Probably density functions for TCS valid for land. a–c, TCS distributions calculated on the basis of 25-year rolling windows: (**a**) for 25-year periods beginning in 1964–1974, (**b**) for 25-year periods beginning in 1975–1985 and (**c**) for all 25-year periods of the 46-year record. **d**, Median (horizontal lines), 25th and 75th percentiles (boxes) and maximum/minimum values for all distributions. Outliers are marked with circles. Note that these TCS estimates are valid for land areas only.

observational studies of TCS yields a wide range, from 0.7 to 3.6 K, but generally central estimates below 2 K (ref. 18). Given that the globe has warmed by approximately 1 K since pre-industrial times, mainly owing to increasing atmospheric CO_2 (ref. 8), TCS estimates below 1 K seem highly implausible. Incidentally, the present study produces a TCS estimate that is identical to the amount of warming that more than 100 countries have adopted as a limit beyond which severe risks and damage due to global warming are thought to ensue[22]. However, recent arguments have been made for an even lower limit of 'acceptable warming' of 1.5 K (ref. 23). One implication of our findings is that warming will exceed this limit by the middle of the present century without a rapid transition to net zero carbon emission worldwide.

The apparent hiatus in global warming observed over the past decade has been the topic of numerous papers in recent years, and its cause and even existence is now being debated[24,25]. Some recent estimates of climate sensitivity that incorporate the most up-to-date observational data sets, including the so-called hiatus, have reported very low climate sensitivities[3,26]. To test the sensitivity of our method to the period selected for analysis, we analysed 25-year subsets of the time period 1964 to 2010, and produced probability density functions (PDFs) for TCS (Fig. 3). Independent of which 25-year time window is selected, the TCS for land lies in the interval 2–4.5 K. The PDFs are relatively broad, with high TCSs typically stemming from 25-year periods of rapid warming and lower values during periods with weak temperature trends. Analyses based on shorter time windows are obviously more susceptible to climate variability, and therefore more likely to produce biased trends. Nevertheless, the PDFs peak at a land TCS of 3–4 K, increasing the confidence in the best estimate from the full 46-year time period. Thus, the observational-based and GCM-independent analysis presented here supports the best TCS estimate and range produced by GCMs, despite incorporating observations from the so-called hiatus, which has caused other observational methods to produce anomalously low TCS estimates. The temperature evolution predicted by our method does not notably diverge from observations during the hiatus period (1998–2010, Fig. 2), suggesting that regions with weak temperature trends also experienced a DSRS decrease during this period, thus hinting at a potential contribution to the hiatus from anthropogenic or volcanic aerosols trends. However, the current prevailing view is that the hiatus can be attributed to variability internal to the climate system, which temporarily causes more heat to mix into the deep ocean via the Equatorial Pacific[27]. Thus, we suggest that observational studies that produce anomalously low climate sensitivities as a result of incorporating the hiatus period are either overly sensitive to temperature trends of the past decade, or alternatively not properly accounting for the effect of aerosols.

Methods

Methods and any associated references are available in the online version of the paper.

Received 22 October 2015; accepted 5 February 2016; published online 14 March 2016

References

1. Collins, M. *et al*. in *Climate Change 2013: The Physical Science Basis* (eds Stocker, T. F. *et al*.) Ch. 12, 1029–1136 (IPCC, Cambridge Univ. Press, 2013).
2. Otto, A. *et al*. Energy budget constraints on climate response. *Nature Geosci.* **6,** 415–416 (2013).
3. Lewis, N. & Curry, J. The implications for climate sensitivity of AR5 forcing and heat uptake estimates. *Clim. Dynam.* **45,** 1009–1023 (2015).
4. Allen, M. R. & Frame, D. J. Call off the quest. *Science* **318,** 582–583 (2007).
5. Padilla, L. E., Vallis, G. K. & Rowley, C. W. Probabilistic estimates of transient climate sensitivity subject to uncertainty in forcing and natural variability. *J. Clim.* **24,** 5521–5537 (2011).
6. Wild, M. Enlightening global dimming and brightening. *Bull. Am. Meteorol. Soc.* **93,** 27–37 (2012).
7. Wild, M. Global dimming and brightening: a review. *J. Geophys. Res.* **114,** D00D16 (2009).
8. Myhre, G. *et al*. in *Climate Change 2013: The Physical Science Basis* (eds Stocker, T. F. *et al*.) Ch. 8, 659–740 (IPCC, Cambridge Univ. Press, 2013).
9. Norris, J. R. & Wild, M. Trends in aerosol radiative effects over Europe inferred from observed cloud cover, solar "dimming" and solar "brightening". *J. Geophys. Res.* **112,** D08214 (2007).
10. Andreae, M. O., Jones, C. D. & Cox, P. M. Strong present-day aerosol cooling implies a hot future. *Nature* **435,** 1187–1190 (2005).
11. Lohmann, U. *et al*. Total aerosol effect: radiative forcing or radiative flux perturbation? *Atmos. Chem. Phys.* **10,** 3235–3246 (2010).
12. Kiehl, J. T. Twentieth century climate model response and climate sensitivity. *Geophys. Res. Lett.* **34,** L22710 (2007).
13. Harris, I., Jones, P. D., Osborn, T. J. & Lister, D. H. Updated high-resolution grids of monthly climatic observations—the CRU TS3.10 Dataset. *Int. J. Climatol.* **34,** 623–642 (2014).
14. Hofmann, D. J. *et al*. The role of carbon dioxide in climate forcing from 1979 to 2004: introduction of the Annual Greenhouse Gas Index. *Tellus B* **58,** 614–619 (2006).
15. Gilgen, H. & Ohmura, A. The global energy balance archive. *Bull. Am. Meteorol. Soc.* **80,** 831–850 (1999).
16. Arellano, M. & Bond, S. Some tests of specification for panel data—Monte-Carlo evidence and an application to employment equations. *Rev. Econ. Stud.* **58,** 277–297 (1991).
17. Kaufmann, R. K., Kauppi, H., Mann, M. L. & Stock, J. H. Reconciling anthropogenic climate change with observed temperature 1998–2008. *Proc. Natl Acad. Sci. USA* **108,** 11790–11793 (2011).
18. Bindoff, N. L. *et al*. in *Climate Change 2013: The Physical Science Basis* (eds Stocker, T. F. *et al*.) Ch. 10, 867–952 (IPCC, Cambridge Univ. Press, 2013).
19. Wild, M., Ohmura, A. & Makowski, K. Impact of global dimming and brightening on global warming. *Geophys. Res. Lett.* **34,** L04702 (2007).
20. Shindell, D. T. Inhomogeneous forcing and transient climate sensitivity. *Nature Clim. Change* **4,** 274–277 (2014).
21. Hartmann, D. L. *et al*. in *Climate Change 2013: The Physical Science Basis* (eds Stocker, T. F. *et al*.) Ch. 2, 159–254 (IPCC, Cambridge Univ. Press, 2013).
22. Meinshausen, M. *et al*. Greenhouse-gas emission targets for limiting global warming to 2 degrees C. *Nature* **458,** 1158–U1196 (2009).
23. Rogelj, J. *et al*. Energy system transformations for limiting end-of-century warming to below 1.5 degrees C. *Nature Clim. Change* **5,** 519–527 (2015).
24. Meehl, G. A., Arblaster, J. M., Fasullo, J. T., Hu, A. X. & Trenberth, K. E. Model-based evidence of deep-ocean heat uptake during surface-temperature hiatus periods. *Nature Clim. Change* **1,** 360–364 (2011).
25. Santer, B. D. *et al*. Volcanic contribution to decadal changes in tropospheric temperature. *Nature Geosci.* **7,** 185–189 (2014).
26. Skeie, R. B., Berntsen, T., Aldrin, M., Holden, M. & Myhre, G. A lower and more constrained estimate of climate sensitivity using updated observations and detailed radiative forcing time series. *Earth Syst. Dynam.* **5,** 139–175 (2014).
27. Kosaka, Y. & Xie, S. P. Recent global-warming hiatus tied to equatorial Pacific surface cooling. *Nature* **501,** 403–407 (2013).
28. Klimont, Z., Smith, S. J. & Cofala, J. The last decade of global anthropogenic sulfur dioxide: 2000–2011 emissions. *Environ. Res. Lett.* **8,** 014003 (2013).
29. Smith, S. J. *et al*. Anthropogenic sulfur dioxide emissions: 1850–2005. *Atmos. Chem. Phys.* **11,** 1101–1116 (2011).

Acknowledgements

This research was supported by an interdisciplinary seed grant awarded by the Yale Climate and Energy Institute (YCEI). P.C.B.P. acknowledges research support from the NSF under Grant No. SES 1258258.

Author contributions

T.S. and P.C.B.P. designed the project. T.L. performed data quality checks and all technical analysis. M.W. and U.L. contributed data and helped with interpretation. T.S. and P.C.B.P. wrote the paper with contributions from all co-authors.

Additional information

Supplementary information is available in the online version of the paper. Reprints and permissions information is available online at www.nature.com/reprints. Correspondence and requests for materials should be addressed to T.S.

Competing financial interests

The authors declare no competing financial interests.

Methods

This study relies on three observational data sets: The Global Energy Balance Archive (GEBA, www.geba.ethz.ch), the Climate Research Unit Time Series (CRU TS, version 3.2, badc.nerc.ac.uk/data/cru) and the National Oceanic and Atmospheric Administration (NOAA) Annual Greenhouse Gas Index (AGGI, http://www.esrl.noaa.gov/gmd/aggi) data sets. The latter provides a global and annual mean time series of equivalent CO_2 concentrations in the atmosphere, which is calculated by taking the radiative forcings associated with changes in all non-CO_2 GHGs and converting them into equivalent changes in atmospheric CO_2 (that is, the CO_2 increase required to produce the same forcing). The GEBA data set reports monthly mean downwelling shortwave radiation (DSRS) reaching the surface, as measured at approximately 2,500 instrumented surface stations worldwide. Out of these, data from only about 1,300 surface stations are selected for the purpose of this study, on the basis of strict criteria on time series length and continuity, as well as data quality control. The availability of high-quality continuous data limited the time period studied here to 1964–2010. For each selected station, i, the annual mean time series of DSRS, denoted R_i, is assigned a corresponding high-resolution temperature time series T_i from CRU TS3.2. The CRU TS3.2 data set is available for download from the British Atmospheric Data Center (BADC) and is provided on a $0.5^\circ \times 0.5^\circ$ horizontal resolution. The third and final data set, AGGI, provides annual and global mean atmospheric abundances for all major well-mixed long-lived greenhouse gases: carbon dioxide, methane, nitrous oxide, CFC-12 and CFC-11, as well as 15 minor halogenated gases from the NOAA global air sampling network. By converting the abundances of all gases other than CO_2 into CO_2 equivalent abundances, the AGGI data set can offer an annual and global mean time series of equivalent CO_2 abundance ($CO_{2,eq}$), which is the time series that is used here. Because these well-mixed GHGs exhibit little spatial variability, the global mean values can be taken as valid for all surface stations[8]. These time series, two of them specific to each of the 1,300 surface stations, and the third offering one single annual value for the entire globe, are incorporated into equations (2) and (3) below, which in combination predict the temperature evolution at individual surface sites[30].

The equations (originally derived in ref. 30) thus describe the annual mean temperature at any given station in year $t+1$ as a function of local and global mean temperatures (T_i and T), local and global mean DSRS, as well as the global mean $CO_{2,eq}$, all for the previous year t. The dependence of local temperature evolution on these variables is justified on the basis of energy balance considerations, but note that we are not explicitly solving an energy balance model here. Instead, the energy balance framework is simply used to identify variables that might be expected to exert an influence on local temperature evolution. Thereafter, the parameters that relate local temperature evolution to these variables are determined entirely by our observed time series, using the following equations:

$$T_{i,t+1} = \beta_1 T_{i,t} + \beta_2 R_{i,t} + \lambda_t + u_{i,t+1} \quad (2)$$

$$\lambda_t = \gamma_0 + \gamma_1 T_t + \gamma_2 R_t + \gamma_3 \log(CO_{2,eq}) \quad (3)$$

where β_1, β_2, γ_0, γ_1, γ_2 and γ_3 are parameters that are constrained by the three-dimensional data sets and $u_{i,t+1}$ is a station-specific idiosyncratic shock. Estimation is performed using dynamic panel data and cointegration methods. The goal is to estimate the parameter values (the β's and γ's) that best describe all observations over time and space in a predictive framework (for $T_{i,t+1}$), allowing for local transient responses (via $\beta_1 T_{i,t}$) to long-run global influences (λ_t) and the presence of stochastic trends in those global forcing factors. Time series nonstationarity and co-movement among the global variable constituents of λ_t is accommodated through the predictive regression form of equation (2) and the use of cointegrating regression and error correction techniques that allow for nonstationarity in the global drivers. In particular, when T_t, R_t and $CO_{2,eq}$ are cointegrated, the time series effect λ_t may be interpreted as a long-run equilibrium global forcing effect that acts as one of the drivers in equation (2). Table 1 shows the parameter values that result from the direct application of dynamic panel methods. Further econometric analysis and discussion is provided below and in Supplementary Tables 1–5. Note that this approach implicitly assumes that there is no long-term trend in Earth's heat capacity, which is dominated by ocean heat uptake.

As expected, at any year the present temperature will be a relatively good predictor of next year's temperature (parameter β_1). The temperature influence of the local DSRS is evident by the fact that β_2 is positive and significantly different from zero—the more incoming solar radiation at the surface, the warmer. The parameter that relates local temperature in year $t+1$ to the station-mean temperature in year t (γ_1) represents two processes: transport of heat to/from the stations from/to the surroundings, as well as the Planck feedback (a warmer land surface loses more energy to space through infrared radiation). The observations suggest that the latter dominates. The parameter relating local temperature to global (that is, station-mean) DSRS (γ_2) is not significantly different from zero, and the observations therefore suggest that the global solar radiation balance does not have a strong influence on local temperature trends. An alternative interpretation is that a significant proportion of the DSRS trend is due to atmospheric black carbon aerosols. Because of the positive forcing that black carbon exerts at the top of the atmosphere, an associated warming would in this case be expected outside major source regions. However, as the impact of the global radiation trend on local temperature is not statistically significant, this could be indicative of a combination of sulfate and black carbon, which causes temperature perturbations due to non-local radiation trends to be small. Finally, $CO_{2,eq}$ has a strong impact on local temperatures, as evident by the positive γ_3, which is significantly different from zero. The value of γ_3 allows for calculations of the TCS through equations (2) and (3). The equations yield the temperature response to a doubling of $CO_{2,eq}$—for example over the pre-industrial value of 280 ppm—as follows: $\Delta T_{2xCO_2} = \gamma_3 \log(560) - \gamma_3 \log(280) = \gamma_3 \log(560/280) = \gamma_3 \log_2$.

Table 1 | Parameter values, standard errors and confidence intervals for the parameters of equations (2) and (3).

Parameter	Value	Standard error	95% confidence interval	Relevant variable
β_1	0.9212	0.0040	(0.9133, 0.9292)	T_i
β_2	0.0127	0.0006	(0.0108, 0.0146)	R_i
γ_1	−0.8438	0.1573	(−1.1611, −0.5266)	T
γ_2^*	0.0025	0.0089	(−0.0154, 0.0205)	R
γ_3	4.4056	0.9892	(2.4107, 6.4005)	$CO_{2,eq}$

*Not statistically significant.

The panel model for local temperature evolution given in equations (2) and (3) is formulated in the predictive regression format[31], where the time-specific variate λ_t captures common global temperature, radiation and greenhouse gas influences on station-specific temperature. These global variables typically manifest evidence of stochastic trend (or autoregressive unit root[32]) behaviour over time, as is known from earlier climate research[17,33,34]. The data used in the present study were tested for evidence of unit roots using augmented Dickey–Fuller (ADF; ref. 35), Phillips–Perron (PP; refs 32,36) and KPSS (ref. 37) tests. The results (which are shown in Supplementary Table 1) are confirmatory of the presence of stochastic trends for all variables, although for variable T the ADF and PP coefficient test results are sensitive to the inclusion of deterministic trends in the regression, favouring trend stationarity in that case.

The spatial panel formulation (equations (2) and (3)) allows for local site dynamic responses (via $\beta_1 T_{i,t}$) to local radiation effects ($R_{i,t}$) while controlling for the time series impact of global climate indicators and forcing agents through the presence of λ_t. Time series nonstationarity, as well as potential cointegration among these global variables, is accommodated by the predictive regression form of the formulation.

When T_t, R_t and $CO_{2,eq}$ are cointegrated, the time-specific effect λ_t may be interpreted as a long-run equilibrium global forcing effect that acts as one of the drivers of the local temperature dynamics in equation (2). This equation then falls within the (spatial panel) framework of error correction mechanisms in econometrics[38]. The site-specific innovations $u_{i,t+1}$ are assumed to be martingale differences with respect to past information and aggregate shocks. (In effect, site-specific individual innovations at time $t+1$ are uncorrelated with aggregate shocks and radiation effects that have occurred up to time t). Since estimation and inference involves spatial averaging as well as temporal averaging, the asymptotic theory is normal, and inference is standard for the parameters in equation (2) (ref. 39). This conclusion holds even when the global variables are themselves cointegrated rather than full rank nonstationary.

Cointegration tests among the global variables were conducted and these are reported in Supplementary Table 2. The residual-based tests used here are the Phillips and Ouliaris[40] coefficient (z) and t-ratio ADF (τ) tests for the presence of unit roots in the residuals from cointegrating regressions among the global variables (details are provided in Supplementary Table 2). Critical values are obtained from MacKinnon[41]. The test results show strong evidence of cointegration among the global variables, and these results are robust to the presence of a deterministic trend in the cointegrating regression. There is also evidence of dyadic cointegration in the pairs (T_t, R_t) and (T_t, $CO_{2,eq}$), the latter corroborating evidence in earlier work[33,34,42].

We considered two extensions that involve model formulation and estimation. First, equations (2) and (3) were formulated to allow for latitudinal coefficient variation. We analysed the impact of latitude on the parameter estimates by parameterizing according to four spatial regions: the Southern Hemisphere (SH, 90° S–15° S), the tropics (Tr, 15° S–15° N), the Northern Hemisphere (NH) subtropics (15° N–45° N), and the NH high latitudes (45° N–90° N). The observations from surface stations in these separate regions are then used to estimate the region-specific parameters. Note that equations (2) and (3) are based on global energy balance considerations, and thus the outcome of applying the

same equations to separate regions, albeit large, must be interpreted with that in mind. The results are reported in Supplementary Table 3. The main features to emerge from these findings are as follows.

First, there is a larger sensitivity to CO_2 at high latitudes than in the tropics, with the NH mid-latitudes yielding the largest γ_3 values. This is consistent with the well-known and expected polar amplification of CO_2 warming.

Second, the parameter values across latitude bands are remarkably consistent, with local radiation effects generally being statistically significant, in contrast with the global radiation effect.

Third, in the tropics and SH, there is a global radiation effect similar in magnitude, but of opposite sign, compared to the local radiation effect. This is suggestive of a significant contribution to dimming from black carbon in this region, which is consistent with the large black carbon sources from biomass burning in the tropics and SH. In the NH, there is no such cancellation, suggesting that cooling aerosols such as sulfate dominate the radiation trends there. This is again consistent with global climate modelling and satellite observations.

Fourth, the NH subtropics and mid-latitudes (15° N–45° N) show the highest sensitivity to trends in DSRS. This is consistent with the findings of ref. 20. The rationale is that NH mid-latitudes have the most land coverage (see Fig. 1b), so the DSRS triggers more rapid land responses and climate feedback mechanisms there than elsewhere.

Finally, the parameter γ_1 is negative everywhere, indicative of the dominant influence of the Planck feedback on this parameter. However, γ_1 is less negative in the NH than in the tropics and SH subtropics (though their confidence intervals overlap), possibly suggesting that increased heat transport from the SH and tropics into the NH extratropics may compensate for some of the extra heat lost to space through infrared radiation as the NH surface warms. This would be consistent with the observation of a southward shift in the Intertropical Convergence Zone (ITCZ) during the second half of the twentieth century, and an associated increased energy flux from the SH to the NH (ref. 43). The ITCZ shift has been attributed to the hemispherically asymmetric cooling effect from anthropogenic aerosols.

The second extension involves the method of estimation. In view of the stochastic trends in the global variables (T_t, R_t, $CO_{2,eq,t}$), the system was re-estimated using dynamic ordinary least squares (DOLS; refs 44–46). This technique includes lead and lag differences in the regression and, as explained in the cited works, provides a convenient linear regression approach for dealing with any error correlation contamination and bias that might arise in nonstationary cointegrating regression. The technique has been used in earlier work by Kaufmann *et al.*[34]. This modification leads to the following reformulation of equations (2) and (3) as

$$T_{i,t+1} = \beta_0 + \beta_1 T_{i,t} + \beta_2 R_{i,t} + \lambda_t + u_{i,t+1} \quad (4)$$

$$\lambda_t = \gamma_0 + \gamma_1 T_t + \gamma_2 R_t + \gamma_3 \ln\left(CO_{2,eq,t}\right) + \boldsymbol{\gamma}_b \cdot \Delta \mathbf{X}_{t-1} + \boldsymbol{\gamma}_c \cdot \Delta \mathbf{X}_{t+1} \quad (5)$$

where $\mathbf{X} = [R, \ln(CO_{2,eq})]$ with corresponding coefficient vectors $\boldsymbol{\gamma}_b = [\gamma_{2,b}, \gamma_{3,b}]$, $\boldsymbol{\gamma}_c = [\gamma_{2,c}, \gamma_{3,c}]$. In this system, as noted above, the time-specific effect λ_t serves as a long run equilibrium error in the global energy balance, an interpretation that is confirmed by unit root tests which strongly reject the presence of a stochastic trend in λ_t (see Supplementary Table 4) and corroborate the finding of cointegration among the trending variables (T_t, R_t, $CO_{2,eq,t}$). Note that equation (4) is formulated with lead differences ΔX_{t+1} and lagged differences ΔX_{t-1} in the primary driver variables X_t, just as in the usual formulation of a DOLS cointegrating regression of T_t on X_t. Equation (4) then falls within the well-studied framework of an error correction mechanism in econometrics[38], although its significance in the present spatial-panel context emerges from the role that the global forcing variables X_t and temperature T_t play in the determination of site-specific dynamics of $T_{i,t+1}$ in equation (4).

The parameter estimates obtained from DOLS regression are given in Supplementary Table 5. The estimates of the global level variable coefficients (γ_1, γ_2, γ_3) and the associated confidence intervals are in each case close to those reported in Table 1. The findings therefore corroborate those from the direct panel regression given without the inclusion of lead and lagged differences, showing that the results are robust to the use of cointegrating methods that allow for the presence of stochastic trends in the data.

Code availability. The code used to generate the parameters of Table 1 and the test results in Supplementary Tables 1–5 are available from the corresponding author on request.

References

30. Magnus, J. R., Melenberg, B. & Muris, C. Global warming and local dimming: the statistical evidence. *J. Am. Stat. Assoc.* **106,** 452–464 (2011).
31. Phillips, P. C. B. Halbert White Jr. Memorial JFEC Lecture: pitfalls and possibilities in predictive regression. *J. Financ. Economet.* **13,** 521–555 (2015).
32. Phillips, P. C. B. Time-series regression with a unit-root. *Econometrica* **55,** 277–301 (1987).
33. Kaufmann, R. K., Kauppi, H. & Stock, J. H. Emissions, concentrations, temperature: a time series analysis. *Climatic Change* **77,** 249–278 (2006).
34. Kaufmann, R. K., Kauppi, H. & Stock, J. H. The relationship between radiative forcing and temperature: what do statistical analyses of the instrumental temperature record measure? *Climatic Change* **77,** 279–289 (2006).
35. Said, S. E. & Dickey, D. A. Testing for unit roots in autoregressive-moving average models of unknown order. *Biometrika* **71,** 599–607 (1984).
36. Phillips, P. C. B. & Perron, P. Testing for a unit-root in time-series regression. *Biometrika* **75,** 335–346 (1988).
37. Kwiatkowski, D., Phillips, P. C. B. & Schmidt, P. Testing for stationarity in the components representation of a time-series. *Economet. Theor.* **8,** 586–591 (1992).
38. Engle, R. F. & Granger, C. W. J. Cointegration and error correction—representation, estimation, and testing. *Econometrica* **55,** 251–276 (1987).
39. Phillips, P. C. B. & Moon, H. R. Linear regression limit theory for nonstationary panel data. *Econometrica* **67,** 1057–1111 (1999).
40. Phillips, P. C. B. & Ouliaris, S. Asymptotic properties of residual based tests for cointegration. *Econometrica* **58,** 165–193 (1990).
41. Mackinnon, J. G. Approximate asymptotic-distribution functions for unit-root and cointegration tests. *J. Bus. Econ. Stat.* **12,** 167–176 (1994).
42. Kaufmann, R. K., Kauppi, H., Mann, M. L. & Stock, J. H. Does temperature contain a stochastic trend: linking statistical results to physical mechanisms. *Climatic Change* **118,** 729–743 (2013).
43. Schneider, T., Bischoff, T. & Haug, G. H. Migrations and dynamics of the intertropical convergence zone. *Nature* **513,** 45–53 (2014).
44. Phillips, P. C. B. & Loretan, M. Estimating long-run economic equilibria. *Rev. Econ. Stud.* **58,** 407–436 (1991).
45. Saikkonen, P. Asymptotically efficient estimation of cointegration regressions. *Economet. Theor.* **7,** 1–21 (1991).
46. Stock, J. H. & Watson, M. W. A simple estimator of cointegrating vectors in higher-order integrated systems. *Econometrica* **61,** 783–820 (1993).